Journal of the Korean Physical Society, Vol. 39, No. 5, November 2001, pp. 0∼0

Comparison of Multilevel Atomic Schemes for SubDoppler Laser Cooling

Soo Chang*
Department of Physics, Hannam University, Taejon 300-791

Taeg Yong Kwon and Ho Seong Lee
Korea Research Institute of Standards and Science, Taejon 305-600

Vladimir G. Minogin
Institute of Spectroscopy, Russian Academy of Sciences, 142190, Troitsk, Moscow Region, Russia

(Received 10 April 2001)

We present the results of the kinetic theory of laser cooling for four basic multilevel atomic schemes: (3+5)-, (5+7)-, (7+9)-, and (9+11)-level atoms in a $\sigma^+ - \sigma^-$ field configuration. The underlying physical processes and the effectiveness of laser cooling are compared for the different models. We show that even-order multiphoton processes caused by two laser waves can be identified as the basic physical mechanism responsible for the subDoppler laser cooling of atoms. The temperature of laser-cooled atoms is derived for all four models and is found to be lower for atomic schemes with bigger numbers of sublevels.

I. INTRODUCTION

In a series of earlier works, we presented a new and quantitative interpretation of the so-called polarization gradient cooling or subDoppler cooling of (3+5)-level atoms by counterpropagating circularly polarized laser waves (*i.e.*, $\sigma^+ - \sigma^-$ configuration) [1,2] or counterpropagating linearly polarized laser waves (*i.e.*, LIN $\perp$ LIN configuration) [3]. Also we developed a new kinetic theory of the magneto-optical trap (MOT) for (3+5)-level atoms in a $\sigma^+ - \sigma^-$ configuration [4,5]. We have shown that in a case of (3+5)-level atoms excited by a $\sigma^+ - \sigma^-$ configuration, a two-photon coherent redistribution of atomic populations results in a sharp narrowing of the velocity distribution of atoms while the subDoppler cooling of (3+5)-level atoms by a LIN $\perp$ LIN configuration is based mainly on a stepwise four-photon process composed of two-photon processes. However, we are still left with the question of what is the quantitative difference between the laser cooling processes applied to different multilevel atomic schemes, such as Na, Rb, Cs and others, which are of use in real experiments. A broader physical interest in comparing laser cooling schemes for different atomic schemes comes from still unclear questions of what is the difference between the elementary excitation processes in different excitation schemes and which scheme leads to the lowest value of atomic temperature. Despite broad use of the subDoppler cooling techniques, the known theoretical studies of laser cooling of atoms do not allow one to compare the efficiency of laser cooling for different atomic schemes [6–11].

In this paper, we present the results of the kinetic theory of laser cooling for four basic multilevel atomic schemes: (3+5)-, (5+7)-, (7+9)-, and (9+11)-level atoms for the same case of a $\sigma^+ - \sigma^-$ cooling field configuration. We compare the underlying physical processes and effectiveness of laser cooling for the different models. The first (3+5)-level scheme may be considered as a pure model scheme described by the total angular momenta $F = 1$ in the ground state and $F' = 2$ in the excited state. The other three schemes can be applied to the cyclic transitions $nS_J(F) - nP_{J+1}(F' = F + 1)$ in ^{23}Na ($n = 3, J = 1/2, F = 2$), ^{87}Rb ($n = 5, J = 1/2, F = 2$), ^{85}Rb ($n = 5, J = 1/2, F = 3$), and ^{133}Cs ($n = 6, J = 1/2, F = 4$). The kinetic theory approach shows that the physical mechanism responsible for subDoppler laser cooling in all the considered schemes is based on two-photon and higher even-order multiphoton transitions between the ground-state sublevels.

II. WIGNER DENSITY MATRIX EQUATIONS

We consider the interaction schemes in Fig. 1. In all schemes the atoms are assumed to be excited by circu-

*E-mail: sjang@mail.hannam.ac.kr

larly polarized laser waves, forming a $\sigma^+ - \sigma^-$ field configuration with respect to the quantization axis Oz. The electric field of the chosen $\sigma^+ - \sigma^-$ field configuration is represented by a composition of two counterpropagating left-circularly polarized waves:

$$\begin{aligned}
&\mathbf{E}(\mathbf{r},t) = \mathbf{E}_1 + \mathbf{E}_2,\\
&\mathbf{E}_1 = \frac{E_0}{2}\left(\mathbf{e}_+ e^{i(kz-\omega t)} - \mathbf{e}_- e^{-i(kz-\omega t)}\right),\\
&\mathbf{E}_2 = \frac{E_0}{2}\left(-\mathbf{e}_+ e^{i(kz+\omega t)} + \mathbf{e}_- e^{-i(kz+\omega t)}\right),
\end{aligned} \qquad (1)$$

where $\mathbf{e}_\pm = \mp\frac{1}{\sqrt{2}}(\mathbf{e}_x \pm i\mathbf{e}_y)$ are the unit spherical vectors, $k = \omega/c$ is the magnitude of the wavevector, and ω is the frequency of the laser waves. With respect to the axis Oz, the first wave is a σ^+ polarized wave, and the second one is a σ^- polarized wave.

We can describe the electric dipole interaction of any $((2F+1)+(2F'+1))$-level atom with the laser field by combining the field representation in Eq. (1) with the density matrix equations in the Wigner representation and the rotating wave approximation [12]. In this paper, we use the Wigner density matrix $\rho_{ab}(\mathbf{r},\mathbf{p},t) = \langle a|\rho(\mathbf{r},\mathbf{p},t)|b\rangle$ defined with respect to the time-dependent atomic eigenfunctions, where $\mathbf{r}$ and $\mathbf{p}$ denote the position and the momentum of the atomic center of mass, respectively. In this representation, the equations for the density matrix elements are

$$\begin{aligned}
i\hbar\frac{d}{dt}\rho_{kl}(\mathbf{r},\mathbf{p}) &= (2\pi)^{-3/2}\sum_m \int V_{km}(\mathbf{q},t)\,\rho_{ml}(\mathbf{r},\mathbf{p}-\frac{1}{2}\hbar\mathbf{q})e^{i\mathbf{q}\cdot\mathbf{r}}d^3q\\
&\quad - (2\pi)^{-3/2}\sum_n \int \rho_{kn}(\mathbf{r},\mathbf{p}+\frac{1}{2}\hbar\mathbf{q})V_{nl}(\mathbf{q},t)\,e^{i\mathbf{q}\cdot\mathbf{r}}d^3q + i\hbar(\Gamma\rho)_{kl},
\end{aligned} \qquad (2)$$

where $d/dt = \partial/\partial t + \mathbf{v}\cdot\nabla$ is the total time (or convective) derivative and the dipole interaction terms are

$$\begin{aligned}
V_{kl}(\mathbf{q},t) &= (2\pi)^{-3/2}\int V_{kl}(\mathbf{r},t)\,e^{-i\mathbf{q}\mathbf{r}}d^3r,\\
V_{kl}(\mathbf{r},t) &= -\mathbf{d}_{kl}\cdot\mathbf{E}(\mathbf{r},t)\,e^{i\omega_{kl}t}.
\end{aligned} \qquad (3)$$

According to the meaning of a rotating wave approximation, the time-harmonic parts (*i.e.*, $\exp[i(\omega-\omega_{kl})t]$) appearing in Eq. (2) are assumed to include the frequency differences only, $|\omega-\omega_{kl}| \ll \omega$.

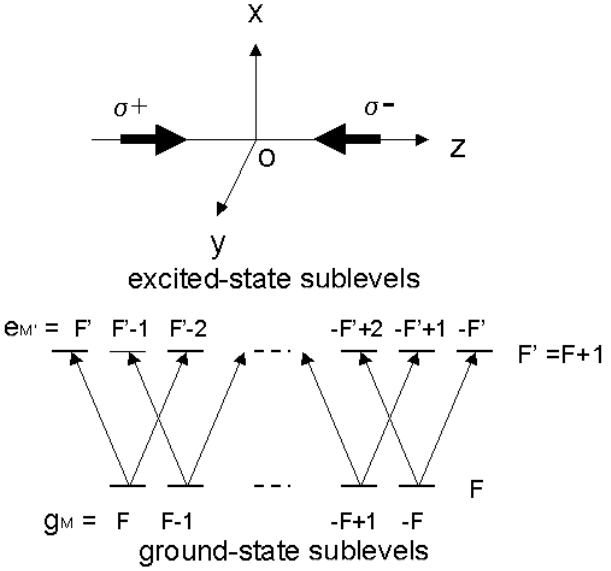

Fig. 1. Schemes of a ((2F+1)-(2F'+1))-level atom excited by counterpropagating circularly polarized laser waves composing a $\sigma^+ - \sigma^-$ field configuration. Arrows show the σ^+ ($g_M \to e_{M+1}$) and σ^- ($g_M \to e_{M-1}$) excitation transitions.

For any dipole interaction scheme shown in Fig. 1 the terms $(\Gamma\rho)_{kl} = \langle k|\Gamma\rho(\mathbf{r},\mathbf{p},t)|l\rangle$ describing the spontaneous relaxation from the excited-state sublevels $|F_eM_e\rangle$ to the ground-state sublevels $|F_gM_g\rangle$ are

$$\begin{aligned}
&\langle F_eM'_e|\Gamma\rho|F_eM_e\rangle = -2\gamma\langle F_eM'_e|\rho|F_eM_e\rangle,\\
&\langle F_eM_e|\Gamma\rho|F_gM_g\rangle = -\gamma\langle F_eM_e|\rho|F_gM_g\rangle,\\
&\langle F_gM'_g|\Gamma\rho|F_gM_g\rangle\\
&\qquad = 2\gamma\sum_{M_eM'_e}\int\left(F_eM_gM'_g\left|\widetilde{A}\right|F_eM_eM'_e\right)\\
&\qquad\quad\times\langle F_eM'_e|\rho(\mathbf{p}+\mathbf{n}\hbar k)|F_eM_e\rangle\,d\Omega,
\end{aligned} \qquad (4)$$

where $d\Omega = \sin(\theta)d\theta d\varphi$ is an elementary solid angle related to the unit vector $\mathbf{n}$ that denotes the direction of the spontaneous photon emission. The integrand in the last line of Eq. (4) is expressed through the Clebsch-Gordan coefficients and the functions $\Phi_\lambda(\mathbf{n})$ describing the angular distribution of the spontaneous emission:

$$\begin{aligned}
&\left(F_eM_gM'_g\left|\widetilde{A}\right|F_eM_eM'_e\right)\\
&\quad = \sum_{\lambda=0,\pm1}(F_gM'_g1\lambda\mid F_eM'_e)\\
&\quad\times(F_gM_g1\lambda\mid F_eM_e)\Phi_\lambda(\mathbf{n}).
\end{aligned} \qquad (5)$$

For circular ($\lambda = \pm1$) and linear ($\lambda = 0$) polarizations, the functions $\Phi_\lambda(\mathbf{n})$ are

$$\Phi_{\pm1}(\mathbf{n}) = \frac{3}{16\pi}\left(1+n_z^2\right), \quad \Phi_0(\mathbf{n}) = \frac{3}{8\pi}\left(1-n_z^2\right), \qquad (6)$$

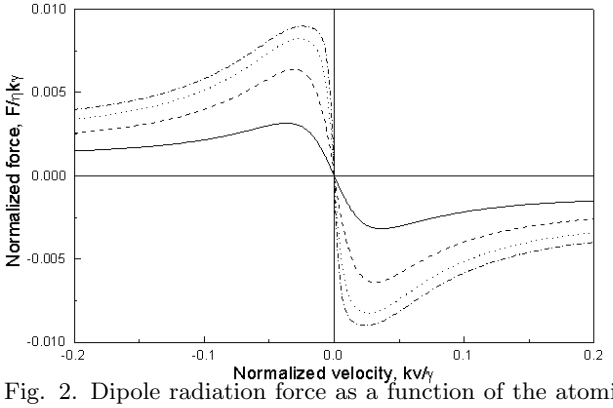

Fig. 2. Dipole radiation force as a function of the atomic velocity $v = v_z$ for a (3+5)-level atom (solid line), a (5+7)-level atom (dashed line), a (7+9)-level atom (dotted line), and a (9+11)-level atom (dash-dotted line) excited by a $\sigma^+ - \sigma^-$ field configuration at a saturation parameter $G = 2\Omega^2/\gamma^2 = 4$ and a detuning $\delta = -20\gamma$.

where n_z is the projection of the unit vector $\mathbf{n}$ on the quantization axis Oz. In the above equations the total spontaneous decay rate from the excited to the ground state is

$$W_{\rm sp} = 2\gamma = \frac{4}{3}\frac{\|d\|^2\omega_0^3}{(2F'+1)\hbar c^3}, \tag{7}$$

where $\|d\| = \langle F'\|d\|F\rangle$ is the reduced dipole matrix element and ω_0 is the atomic transition frequency. We have also defined the Rabi frequency Ω for multilevel atoms as

$$\Omega = \frac{\|d\|E_0}{2\sqrt{2F'+1}\hbar}. \tag{8}$$

Complete sets of density matrix equations consist of 34 equations for a (3+5)-level atom, 74 equations for a (5+7)-level atom, 130 equations for a (7+9)-level atom, and 202 equations for a (9+11)-level atom. Specific examples of the density matrix equations for a (9+11)-level atom are

$$\begin{aligned}
\frac{d}{dt}\rho_{g_0g_0} &= i\frac{\Omega}{\sqrt{3}}\left(e^{ikz}\rho^{(-)}_{e_{-1}g_0} + e^{-ikz}\rho^{(+)}_{e_{+1}g_0}\right)e^{i\delta t} + \text{c.c.} \\
&\quad + 2\gamma\left(\frac{1}{3}\left\langle\rho^{-1}_{e_{-1}e_{-1}}\right\rangle + \frac{5}{9}\left\langle\rho^{0}_{e_0e_0}\right\rangle + \frac{1}{3}\left\langle\rho^{1}_{e_1e_1}\right\rangle\right), \\
\frac{d}{dt}\rho_{g_{-1}g_1} &= i\sqrt{\frac{7}{15}}\Omega\left(e^{i\delta t}\rho^{(-)}_{e_{-2}g_1} - e^{-i\delta t}\rho^{(+)}_{g_{-1}e_2}\right)e^{ikz} \\
&\quad + i\sqrt{\frac{2}{9}}\Omega\left(e^{i\delta t}\rho^{(+)}_{e_0g_1} - e^{-i\delta t}\rho^{(-)}_{g_{-1}e_0}\right)e^{-ikz} \\
&\quad + 2\gamma\left(\frac{\sqrt{210}}{45}\left\langle\rho^{-1}_{e_{-2}e_0}\right\rangle + \frac{8}{15}\left\langle\rho^{0}_{e_{-1}e_1}\right\rangle\right. \\
&\quad \left. + \frac{\sqrt{210}}{45}\left\langle\rho^{1}_{e_0e_2}\right\rangle\right), \\
\frac{d}{dt}\rho_{g_1e_2} &= -i\sqrt{\frac{7}{15}}\Omega\left(\rho^{(-)}_{g_1g_1} - \rho^{(+)}_{e_2e_2}\right)e^{-ikz+i\delta t} \\
&\quad - i\Omega\left(\frac{1}{\sqrt{15}}\rho^{(+)}_{g_1g_3} - \sqrt{\frac{2}{9}}\rho^{(-)}_{e_0e_2}\right)e^{ikz+i\delta t} - \gamma\rho_{g_1e_2},
\end{aligned} \tag{9}$$

where the detuning of the laser field frequency with respect to the atomic transition frequency is defined by $\delta = \omega - \omega_0$. In the above, we have also used the short notation

$$\begin{aligned}
\rho^{(\pm)}_{ab} &= \langle a\left|\rho\left(\mathbf{r}, \mathbf{p} \pm \frac{1}{2}\hbar\mathbf{k}, t\right)\right| b\rangle, \\
\left\langle\rho^{\lambda}_{e_{M'}e_{M''}}\right\rangle &= \int \Phi_\lambda(\mathbf{n})\,\rho^{(\mathbf{n})}_{e_{M'}e_{M''}}d\Omega, \\
\rho^{(\mathbf{n})}_{e_{M'}e_{M''}} &= \langle e_{M'}\left|\rho\left(\mathbf{r}, \mathbf{p} + \mathbf{n}\hbar k, t\right)\right| e_{M''}\rangle,
\end{aligned} \tag{10}$$

where we let $\mathbf{k} = k\mathbf{e}_z$ and $a, b = g_M$ or $e_{M'}$.

III. FOKKER-PLANCK EQUATIONS

Assuming the usual condition that the atom-laser field interaction time $\tau_{\rm int}$ exceeds both the spontaneous decay time $\tau_{\rm sp} = 1/2\gamma$ and any other characteristic times $\tau_{\rm rel}$ which define the relaxation of the internal atomic states, $\tau_{\rm int} \gg \tau_{\rm sp}, \tau_{\rm rel}$, we transform the density matrix equations for every atomic scheme shown in Fig. 1 to the Fokker-Planck kinetic equations by following the basic steps already described in Refs. 1 and 2. At the first step, the density matrix elements are expanded in powers of the photon momentum $\hbar k$. At the next step, the explicit time dependence is eliminated from the equations by proper substitutions for the off-diagonal density-matrix elements. In particular, the off-diagonal optical coherences are replaced by

$$\rho_{g_Me_{M+1}} = \sigma_{g_Me_{M+1}}e^{-ikz+i\delta t},$$

and the off-diagonal symmetric ground-state coherences by

$$\rho_{g_{-M}g_M} = \sigma_{g_{-M}g_M}e^{-i2Mkz}.$$

After that, the quantities ρ_{aa} and σ_{ab} are considered as functionals of the Wigner quasi-probability distribution function,

$$w = \sum_M \rho_{g_Mg_M} + \sum_{M'}\rho_{e_{M'}e_{M'}}, \tag{11}$$

which is assumed to be properly normalized.

The functional dependence is represented as an expansion with respect to the photon momentum,

$$\rho_{ab} = R^0_{ab}w + \hbar kS^1_{ab}\frac{\partial w}{\partial p_z} + \dots, \tag{12}$$

where the unknown diagonal functions satisfy the normalization conditions

$$\sum R^0_{aa} = 1,\ \sum S^1_{aa} = 0, \dots \tag{13}$$

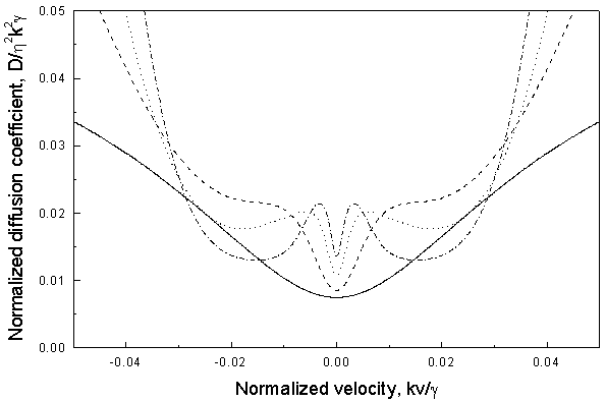

Fig. 3. Diffusion coefficient $D = D_{zz}$ as a function of the velocity for a (3+5)-level atom (solid line), a (5+7)-level atom (dashed line), a (7+9)-level atom (dotted line), and a (9+11)-level atom (dash-dotted line) at the same parameters as in Fig. 2.

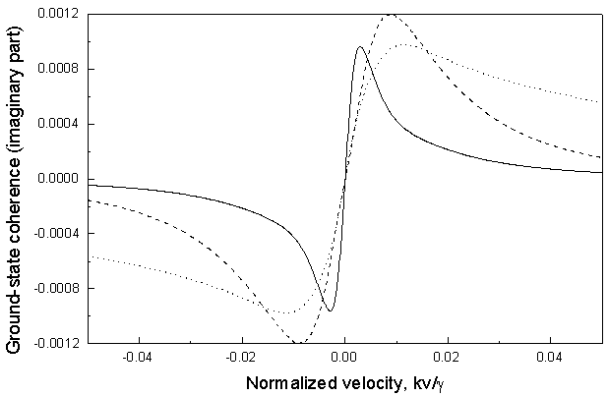

Fig. 4. Imaginary parts of the ground-state coherence $R^o_{g_{-3}g_3}$ (solid line), $R^o_{g_{-2}g_2}$ (dashed line), and $R^o_{g_{-1}g_1}$ (dotted line) as functions of the velocity for a (7+9)-level atom excited by a $\sigma^+ - \sigma^-$ field configuration at the same parameters as in Fig. 2.

and $a, b = g_M$ or $e_{M'}$. The conditions in Eq. (13) follow directly from the definition of the Wigner quasi-probability distribution function in Eq. (11).

Substitution of the general solution, Eq. (12), into the equations for the expanded Wigner density matrix elements finally gives the kinetic equation that governs the time evolution of the distribution function $w = w(\mathbf{r}, \mathbf{p}, t)$. To second order in the photon momentum $\hbar k$, the kinetic equation for the function $w = w(\mathbf{r}, \mathbf{p}, t)$ reduces to the Fokker-Planck equation

$$\frac{dw}{dt} = -\frac{\partial}{\partial p_z}(Fw) + \sum \frac{\partial^2}{\partial p_i^2}(D_{ii} w), \qquad (14)$$

where $i = x, y, z$, $F = F_z$ is the dipole radiation force, and D_{ii} is the momentum diffusion tensor.

IV. RADIATION FORCE, DIFFUSION TENSOR, ATOMIC TEMPERATURE

The velocity dependence of the dipole radiation force for the four considered atomic schemes is shown in Fig. 2. For any of these schemes, the dipole radiation force includes a narrow structure located at zero velocity. For a negative detuning, any force at small velocities reduces to the friction force, $F = -m\beta v$, $v = v_z$, where the friction coefficient is given by $\beta = -[dF/d(mv)]_{v=0}$. The slope of the force near zero velocity, which defines the friction coefficient β, increases when the number of levels increases. The diffusion coefficient $D = D_{zz}$ as a function of velocity shows a narrow dip located at zero velocity. Starting from a (5+7)-level atom these dips exhibit additional narrow structures, which are most clearly seen for the (7+9)- and the (9+11)-level atoms (Fig. 3).

The behaviors of the force and the diffusion coefficient in the kinetic equation, Eq. (14), have a natural explanation in terms of the atomic coherences and populations. As was explained in previous papers [1,2], in the case of a (3+5)-level atom excited by a $\sigma^+ - \sigma^-$ configuration, the narrow resonance structures come from the two-photon process that connects the ground-state sublevels $|g_{-1}\rangle$ and $|g_1\rangle$. In cases of more complicated atomic schemes, higher even-order multiphoton processes give additional contributions to the ground-state coherences and populations. As a specific example, Fig. 4 shows the imaginary parts of the ground-state coherences $R^0_{g_{-M}g_M}$, $M = 1, 2, 3$ (see Eq. (12)) for a (7+9)-level atom. In the case of a (7+9)-level scheme, three basic multiphoton processes exist: the two-photon process contributing to the ground-state coherence $R^0_{g_{-1}g_1}$, the four-photon process contributing to the ground-state coherence $R^0_{g_{-2}g_2}$, and the six-photon process contributing to the ground-state coherence $R^0_{g_{-3}g_3}$. According to Fig. 4, the lowest-order two-photon process gives the broadest velocity structure, the next four-photon process a medium width structure, and the highest six-photon process the narrowest structure. The narrowest structure is accordingly responsible for the slope in the force at zero velocity, *i.e.*, for the friction coefficient for a (7+9)-level atom. In a similar way, the narrowest structure is responsible for the fine structure of the velocity dip in the diffusion coefficient for a (7+9)-level atom (Fig. 3). The same general explanation can be provided for any other atomic scheme as shown in Fig. 1.

The narrow velocity structures caused by the multiphoton transitions exist naturally in any atomic function related to the ground-state coherences. In particular, every ground-state atomic population $R^0_{g_M g_M}$ includes narrow multiphoton velocity structures though their contributions depend on the magnetic sublevel as can be seen in a case of a (9+11)-level atom (Fig. 5). Physically, the contributions of the multiphoton processes are most clearly exhibited in the central ground-state populations $R^0_{g_0 g_0}$ which are less perturbed by the optical pumping

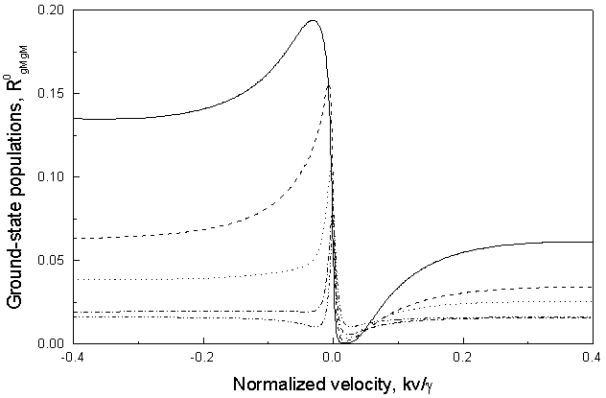

Fig. 5. Ground-state populations $\frac{1}{4}R^0_{g_4g_4}$ (solid line), $R^0_{g_3g_3}$ (dashed line), $R^0_{g_2g_2}$ (dotted line), $R^0_{g_1g_1}$ (dash-dotted line), and $R^0_{g_0g_0}$ (dash-double dotted line) for a (9+11)-level atom as functions of the velocity at the same parameters as in Fig. 2.

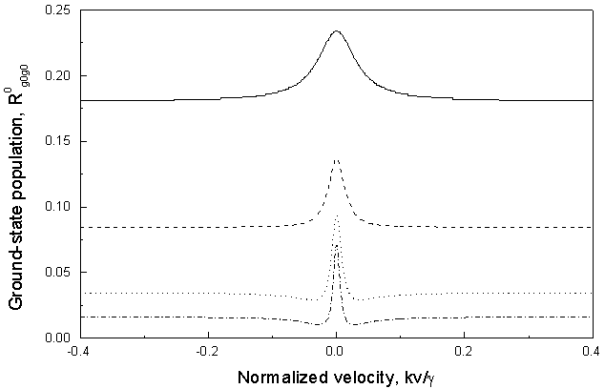

Fig. 6. Ground-state population $R^0_{g_0g_0}$ as a function of the velocity for a (3+5)-level atom (solid line), a (5+7)-level atom (dashed line), a (7+9)-level atom (dotted line), and a (9+11)-level atom (dash-dotted line) at the same parameters as in Fig. 2.

processes in the low velocity region. The velocity dependence of the central atomic population for different atomic schemes is shown in Fig. 6. As can be seen, the velocity width of the ground-state population $R^0_{g_0g_0}$ (see Eq. (12)) reduces from a (3+5)-level scheme to a (9+11)-level scheme, reflecting the increasing role of the higher-order multiphoton processes.

Qualitatively, the contribution of any even-order multiphoton process is similar to the contribution of a two-photon process in the simplest case of a (3+5)-level atom. Any even-order multiphoton process is effective at zero velocity. In the atom's rest frame, the absorption of n photons from one travelling wave with polarization $\sigma^{\pm}$ and the emission of n photons into the other counterpropagating travelling wave with polarization $\sigma^{\mp}$ results in a $2n$-photon transition between the ground-state sublevels. According to the energy conservation law, this process does not change the atom's energy, $n(\omega \pm kv) - n(\omega \mp kv) = 0$. The last equation, thus, directly proves that any $2n$-photon resonance structure is located at zero velocity, $kv = 0$. The frequency and the velocity widths of the different $2n$-photon processes can be shown to depend on the contributions of the odd-order multiphoton processes connecting the ground-state sublevels with the excited-state sublevels. Since the ground-state sublevels have zero width, the total effective frequency width of every even-order resonance is defined by the effective width of the upper-state sublevels $\delta\omega$. For a greatly detuned laser field, $|\delta| \gg \gamma$, the last quantity is defined, as usual, by the rate of the one-photon transitions, $\delta\omega \simeq \gamma\Omega^2/\delta^2$. This quantity defines, accordingly, the frequency width of the 2-photon processes for any atomic scheme. In a similar way, every $2n$-photon resonance is most effective when the total width of the $2n$-photon process, $n(\delta\omega)_{2n}$, is about the total effective width, $n(\delta\omega)_{2n} \simeq \delta\omega$. Accordingly, the resonance frequency region for a $2n$-photon process is about $(\delta\omega)_{2n} \simeq \delta\omega/n$, and the velocity region is about $(\delta v)_{2n} \simeq (\delta\omega/k)/n$. The frequency and the velocity widths of the $2n$-photon process are, thus, approximately inversely proportional to the order of the process. This qualitative conclusion is in agreement with the dependence of the velocity width of the $2n$-photon resonance on the order of resonance, as can be seen in Fig. 4 for the case of the (7+9)-level atom. For different atomic schemes, the widths $(\delta v)_{2F}$ of the highest order resonances are defined by the same estimate and, thus, follow the dependence $(\delta v)_{2F} \simeq (\delta\omega/k)/F$, which is in qualitative agreement with the data shown in Fig. 6.

It is to be stressed that the comparisons of the physical quantities made above for the different atomic schemes were in terms of a universally defined dimensionless saturation parameter $G = 2\Omega^2/\gamma^2$. For any practical purpose, the saturation parameter can equivalently be represented as $G = I/I_{\rm S}$, where $I = (c/8\pi)E_0^2$ is the intensity of a single travelling wave with polarization σ^+ or σ^- and $I_{\rm S} = \hbar\gamma\omega_0^3/6\pi c^2$ is the saturation intensity, does not explicitly depend on the quantum numbers of the atomic scheme.

Figures 7 and 8 show the dependences of the atomic temperature on the value of the negative detuning and the saturation parameter for the above four atomic schemes. The atomic temperature is defined, as usual, by the Einstein relation $T = D(0)/M\beta k_{\rm B}$, where $D(0)$ is the diffusion coefficient at zero velocity, M is the atomic mass, and $k_{\rm B}$ is the Boltzmann constant. For any given atomic scheme, the value of the temperature decreases with increasing detuning and decreasing saturation parameter. For different schemes, the temperature is approximately inversely proportional to the number of atomic levels. All the above features of the temperature behavior reflect the contributions of the multiphoton processes responsible for the friction coefficient and the diffusion coefficient at zero velocity.

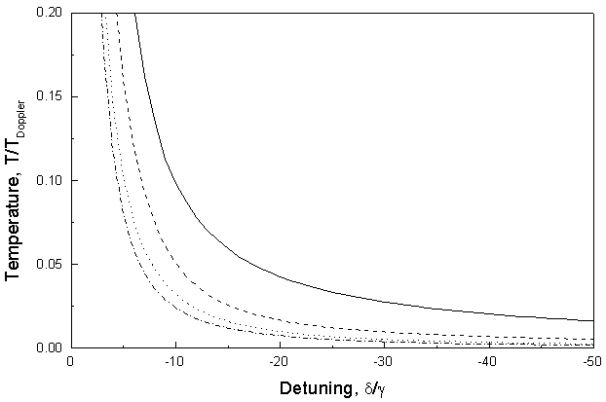

Fig. 7. Atomic temperature as a function of detuning for a (3+5)-level atom (solid line), a (5+7)-level atom (dashed line), a (7+9)-level atom (dotted line), a (9+11)-level atom (dash-dotted line) excited by a $\sigma^+ - \sigma^-$ field configuration at a saturation parameter $G = 4$. The temperature is in the unit of the Doppler temperature $T_{\rm Doppler} = \hbar\gamma/k_{\rm B}$.

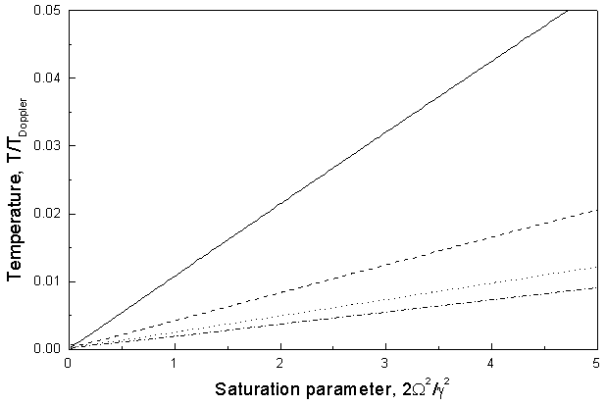

Fig. 8. Atomic temperature as a function of the saturation parameter for a (3+5)-level atom (solid line), a (5+7)-level atom (dashed line), a (7+9)-level atom (dotted line), and a (9+11)-level atom (dash-dotted line) for detuning $\delta = -20\gamma$.

In general, the cooled temperature at large detuning is defined by an effective light shift of the ground-state sublevels. The value of the light shift, $\delta E \sim \hbar\Omega^2/|\delta|$, defines an approximate value of the atomic translational energy and, accordingly, the value of atomic temperature [6]. For the simplest (3+5)-level atomic scheme, which exhibits two-photon transitions, the quantitative estimate of the atomic temperature is very close to the above estimate [2].

A rough estimate of the dependence of the atomic temperature on the number of atomic levels can be done by assuming a uniform distribution of atoms over the magnetic sublevels. Under this assumption, the above basic estimate for the light shift should be decreased approximately by $2F$ times to give an estimate for the translational atomic energy and, accordingly, the temperature:

$$k_{\rm B}T \sim \hbar\frac{\Omega^2}{2F\,|\delta|} = \frac{\hbar\gamma}{4F}\frac{G\gamma}{|\delta|}. \qquad (15)$$

This estimate is in a good qualitative agreement with data shown in Figs. 7 and 8. Formally, the dependence of the temperature on the ground-state degeneracy can be seen from the Einstein relation. Since the multiphoton processes decrease the velocity widths of the highest-order even resonances by F times, they increase the friction coefficient and decrease the temperature also by F times.

V. CONCLUSION

A comparison of four different atomic schemes shows that the even-order multiphoton processes constitute the basic physical mechanism responsible for the subDoppler laser cooling of atoms. For any atomic scheme considered, even-order multiphoton processes modify the atomic populations at zero velocity, produce narrow velocity structures in atomic coherences, and enhance the slope of the radiation force at zero velocity, leading to the subDoppler laser cooling mechanism. In the case of a (3+5)-level atom the two-photon process gives a basic contribution to the friction force and the diffusion coefficient at low velocity while for a (5+7)-level scheme, the basic contribution comes from the four-photon process. In a similar way, the six-photon process plays the main role in a (7+9)-level atom, and the eight-photon process plays the main role in a (9+11)-level atom. It should be stressed that the same physical origin of the basic processes responsible for the subDoppler laser cooling of atoms in a $\sigma^+ - \sigma^-$ configuration determines the atomic temperature which scales approximately inversely proportional to the order of the multiphoton process. We, thus, conclude that at a given large detuning, the lowest temperature is attained for the atomic scheme which includes the highest number of magnetic sublevels and, thus, exhibits the highest-order multiphoton transitions. The results of our analysis also show that the multiphoton processes may be the basic processes which define the operation of the dipole traps and magneto-optical traps for multilevel atomic schemes. In particular, in the case of the magneto-optical trap with $\sigma^+ - \sigma^-$ field configurations [4,5], multiphoton processes can simultaneously define both the subDoppler cooling of atoms and the shape of the potential well.

ACKNOWLEDGMENTS

This work was supported in part by the Natonal Research Laboratory Project of the Korea Ministry of Science and Technology and by the Russian Fund for Basic Research, grant 99-02-16215.

REFERENCES

[1] S. Chang, T. Y. Kwon, Ho S. Lee, and V. G. Minogin, Phys. Rev. A **60**, 2308 (1999).
[2] S. Chang, T. Y. Kwon, Ho S. Lee, and V. G. Minogin, Phys. Rev. A **60**, 3148 (1999).
[3] S. Chang, T. Y. Kwon, Ho S. Lee, and V. G. Minogin, Phys. Rev. A, to be published (2001).
[4] J. W. Jun, S. Chang, T. Y. Kwon, Ho S. Lee, and V. G. Minogin, Phys. Rev. A **60**, 3960 (1999).
[5] J. W. Jun, S. Chang, T. Y. Kwon, Ho S. Lee, V. G. Minogin, and W. H. Jhe, Phys. Rev. A **60**, 4738 (1999).
[6] J. Dalibard and C. Cohen-Tannoudji, J. Opt. Soc. Am. B **6**, 2023 (1989).
[7] P. J. Ungar, D. S. Weiss, E. Riis, and S. Chu, J. Opt. Soc. Am. B **6**, 2058 (1989) .
[8] K. Mølmer, Phys. Rev. A **44**, 5820 (1991).
[9] G. Nienhuis, P. van der Straten, and S-Q. Shang, Phys. Rev. A **44**, (1991) 462.
[10] *Laser Manipulation of Atoms and Ions.* in *Proceedings of the International School of Physics, Enrico Fermi* (North-Holland, New York, 1992).
[11] M. Drewsen, Ph. Laurent, A. Nadir, G. Santarelli, A. Clairon, Y. Castin, D. Grison, and C. Salomon, Appl. Phys. B **59**, 283 (1994).
[12] V. G. Minogin and V. S. Letokhov, *Laser Light Pressure on Atoms* (Gordon and Breach, New York, 1987).